Transition to turbulence in a shear flow

Bruno Eckhardt[1] and Alois Mersmann[2]
[1]*Fachbereich Physik, Philipps Universität Marburg, D-35032 Marburg, Germany*
[2]*Fachbereich Physik und Institut für Chemie und Biologie des Meeres, C.v. Ossietzky Universität, Postfach 25 03, D-26111 Oldenburg, Germany*
(Received 27 August 1997; revised munuscript received 16 February 1999)

We analyze the properties of a 19-dimensional Galerkin approximation to a parallel shear flow. The laminar flow with a sinusoidal shape is stable for all Reynolds numbers Re. For sufficiently large Re additional stationary flows occur; they are all unstable. The lifetimes of finite amplitude perturbations shows a fractal dependence on amplitude and Reynolds number. These findings are in accord with observations on plane Couette flow and suggest a universality of this transition scenario in shear flows. [S1063-651X(99)02907-4]

PACS number(s): 47.20.Ft, 47.20.Ky, 47.15.Fe, 05.45.−a

I. INTRODUCTION

In many flows the transition to turbulence proceeds via a sequence of bifurcations to flows of ever increasing spatial and temporal complexity. Analytical and experimental efforts, in particular, on layers of fluid heated from below [1,2] and fluids between rotating concentric cylinders [2,3] have lead to the identification and verification of several routes to turbulence that typically involve a transition from a structureless laminar state to a stationary spatially modulated one and then to more complicated states in secondary and higher bifurcations.

Transitions in shear flows do not seem to follow this pattern [4]. Typically, a transition to a turbulent state can be induced for sufficiently large Reynolds number with finite amplitude perturbations, just as in a subcritical bifurcation. However, in the most spectacular cases of plane Couette flow between parallel plates and Hagen-Poiseuille flow in a pipe [5], there is no linear instability of the laminar profile for any finite Reynolds number that could give rise to a subcritical bifurcation. The turbulent state seems to be high dimensional immediately, without clear temporal or spatial patterns (unlike the rolls in Rayleigh-Bénard flow). And the transition seems to depend sensitively on the initial conditions. Based on these characteristic features it has been argued that a transition to turbulence different from the well-known three low-dimensional ones is at work [6].

Recent activity has focused on three features of this transition: the non-normality of the linear eigenvalue problem [6–11], the occurrence of stationary states without instability of the linear profile [12–15], and the fractal properties of the lifetime landscape of perturbations as a function of amplitude and Reynolds number [16]. The non-normality of the linear stability problem implies that even in the absence of exponentially growing eigenstates, perturbations can first grow in amplitude before decaying since the eigenvectors are not orthogonal. During the decay other perturbations could be amplified, giving rise to a noise-sustained turbulence [17]. The amplification could also cause random fluctuations to grow to a size where the nonlinear terms can no longer be neglected [10,11]. Then the dynamics including the nonlinear terms could belong to an asymptotic state, different from the laminar profile, perhaps a turbulent attractor. Presumably, this attractor would be built around stationary or periodic solution. Here, the observation of tertiary structures [12–15] comes in since they could form the basis for the turbulent state. Finally, the observation of fractality in the lifetime distribution suggests that the turbulent state is not an attractor but rather a repeller: Infinite lifetimes occur only along the stable manifolds of the repeller, all other initial conditions will eventually decay. Permanent turbulence would thus correspond to noise-induced excitations onto a repeller.

In plane Couette flow some of the features described above have been identified, but only with extensive numerical effort [12–14,16]. The aim of the present paper is to present a simple model that is based on the Navier-Stokes equation and captures the essential elements of the transition. It is motivated in part by the desire to obtain a numerically more accessible model that perhaps will provide as much insight into the transition as the Lorenz model [18] for the case of fluids heated from below (presumably at the price of similar shortcomings). The two and three degree of freedom models proposed by various groups (and reviewed in [19]) to study the effects of non-normality mock some features of the Navier-Stokes equations considered essential by their inventors but they are not derived in some systematic way from the Navier Stokes equation. The model used here differs from the one proposed by Waleffe [10] in the selection of modes.

Attempts to build models for shear flows using Fourier modes immediately reveal an intrinsic difficulty: In the case of fluids heated from below the nonlinearity arises from the coupling of the temperature gradient to the flow field so that two wave vectors, $\mathbf{k}$ and $2\mathbf{k}$, suffice to obtain nonlinear couplings. In shear flows, the nonlinearity has to come from the coupling of the flow field with itself through the advection term $(\mathbf{u}\cdot\nabla)\mathbf{u}$. This imposes rather strong constraints on the wave vectors. At least three wave vectors satisfying the triangle relation $\mathbf{k}_1+\mathbf{k}_2+\mathbf{k}_3=\mathbf{0}$ are required to collect a contribution from the advection term. A minimal model thus has at least six complex variables. Three of these decay monotonically to zero, leaving three for a nontrivial dynamics. In the subspaces investigated (B.E., unpublished), the most complex behavior found is a perturbed pitchfork bifurcation, which may be seen as a precursor of the observed dynamics:

for Reynolds numbers below a critical value, there is only one stable state. Above that value a pair of stable and unstable states is born in a saddle-node bifurcation. The stable state can be excited through perturbations of sufficient amplitude. The basins of attraction of the two stable states are intermingled, but the boundaries are smooth.

Thus more wave vectors are needed and they have to couple in a nontrivial manner to sustain permanent dynamics. The specific set of modes used is discussed in Sec. II. It is motivated by boundary conditions for the laminar profile and the observation that wave vectors pointing to the vortices of hexagons satisfy the triangle conditions in a most symmetrical manner. Other than that the selected vectors are a matter of trial and error. In the end we arrive at a model with 19 real amplitudes, 2 force terms, and 212 quadratic couplings. Without driving and damping the dynamics is energy conserving, as would be the corresponding Euler equation (suitably truncated). Moreover, the perturbation amplitudes can be put together to give complete flow fields. Thus the model has a somewhat larger number of degrees of freedom, but the dynamics should provide a realistic approximation to shear flows.

The outline of the paper is as follows. In Sec. II we present the model, in particular the selected wave vectors, the equations of motion, and a discussion of symmetries. In Sec. III we focus on the dynamical properties of initial perturbations as a function of amplitude and Reynolds number. In Sec. IV we discuss the stationary states, their bifurcations, and their stability properties. We conclude in Sec. V with a summary and a few final remarks.

II. THE MODEL SHEAR FLOW

Ideal parallel shear flows have infinite lateral extension. Both in experiment and theory this cannot be realized. We, therefore, follow the numerical tradition and chose periodic boundary conditions in the flow and neutral direction. The flow is confined by parallel walls a distance d apart. A convenient way to build a low-dimensional model is to use a Galerkin approximation. Solid boundaries would require the vanishing of all velocity components and complicated Galerkin functions where all the couplings can only be calculated numerically. However, under the assumption that here as well as in many other situations the details of the boundary conditions effect the results only quantitatively but not qualitatively, we can adopt free-free boundary conditions on the walls and use simple trigonometric functions as a basis for the Galerkin expansion. Similarly, the nature of the driving (pressure, boundary conditions, or volume force) should not be essential so that we take a volume force proportional to some basis function (or a linear combination thereof). This still leaves plenty of free parameters to be fixed below.

A. Galerkin approximation

We expand the velocity field in Fourier modes,

$$\mathbf{u}(\mathbf{x},t)=\sum_{\mathbf{k}}\mathbf{u}(\mathbf{k},t)e^{i\mathbf{k}\cdot\mathbf{x}}. \tag{1}$$

Incompressibility demands

$$\mathbf{u}(\mathbf{k},t)\cdot\mathbf{k}=0. \tag{2}$$

The Navier-Stokes equation for the amplitudes $\mathbf{u}(\mathbf{k},t)$ becomes

$$\partial_t\mathbf{u}(\mathbf{k},t)=-ip_{\mathbf{k}}\mathbf{k}-i\sum_{\mathbf{p}+\mathbf{q}=\mathbf{k}}[\mathbf{u}(\mathbf{p},t)\cdot\mathbf{q}]\mathbf{u}(\mathbf{q},t)-\nu\mathbf{k}^2\mathbf{u}(\mathbf{k},t)+f_{\mathbf{k}}, \tag{3}$$

where $p_{\mathbf{k}}$ are the Fourier components of the pressure (divided by the density), ν is the kinematic viscosity, and $f_{\mathbf{k}}$ are the Fourier components of the volume force sustaining the laminar profile.

There are three constraints on the components $\mathbf{u}(\mathbf{k})$: incompressibility (2), reality of the velocity field,

$$\mathbf{u}(-\mathbf{k})=\mathbf{u}(\mathbf{k})^*, \tag{4}$$

and the boundary conditions that the flow is limited by two parallel, impenetrable plates. The ensuing requirement $u_z(x,y,z)=0$ at $z=0$ and $z=d$ (where d is the separation between plates) is most easily implemented through periodicity in z and the mirror symmetry,

$$\begin{pmatrix}u_x\\u_y\\u_z\end{pmatrix}(x,y,-z)=\begin{pmatrix}u_x\\u_y\\-u_z\end{pmatrix}(x,y,z), \tag{5}$$

which, in Fourier space, requires

$$\begin{pmatrix}u_x\\u_y\\u_z\end{pmatrix}(-k_x,-k_y,k_z)=\begin{pmatrix}u_x^*\\u_y^*\\-u_z^*\end{pmatrix}(k_x,k_y,k_z). \tag{6}$$

This is not sufficient to fix the coefficients: the dynamics also has to stay in the relevant subspace, and thus the time derivatives have to satisfy similar requirements.

B. The wave vectors

The choice of wave vectors is motivated by the geometry of the flow and the aim to include nonlinear couplings. The basic flow shall be a flow in the y direction, neutral in the x direction, and sheared in the z direction. Thus we take the first three wave vectors in the z direction,

$$\mathbf{k}_1=\begin{pmatrix}0\\0\\1\end{pmatrix},\qquad\mathbf{k}_2=\begin{pmatrix}0\\0\\2\end{pmatrix},\qquad\mathbf{k}_3=\begin{pmatrix}0\\0\\3\end{pmatrix}. \tag{7}$$

The negative vectors $-\mathbf{k}_i$ also belong to the set but will not be numbered explicitly. In these units, the periodicity in the z direction is 2π, so that the separation between the plates is $d=\pi$ because of the mirror symmetry (5). The amplitude $\mathbf{u}(\mathbf{k}_1)$ will carry the laminar profile and $\mathbf{u}(\mathbf{k}_3)$ can be excited as a modification to the laminar profile. $\mathbf{k}_2$ is needed to provide couplings through the nonlinear term. These three vectors satisfy a triangle identity $\mathbf{k}_1+\mathbf{k}_2-\mathbf{k}_3=0$, but the nonlinear term vanishes since they are parallel.

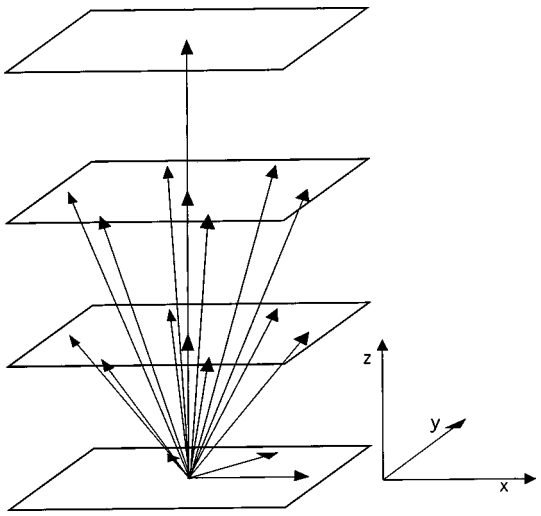

FIG. 1. The 19 wave vectors $\mathbf{k}_1, \ldots, \mathbf{k}_{19}$. The full set is obtained by complementing with $-\mathbf{k}_i$. Thus, there are only three vectors on the symmetry plane $z=0$, six each on the two levels above and a single one on the third plane with $k_z=3$.

The next set of wave vectors contains modulations in the flow and neutral direction,

$$\mathbf{k}_4=\begin{pmatrix}1\\0\\0\end{pmatrix},\quad \mathbf{k}_5=\begin{pmatrix}1/2\\\sqrt{3}/2\\0\end{pmatrix},\quad \mathbf{k}_6=\begin{pmatrix}1/2\\-\sqrt{3}/2\\0\end{pmatrix}. \tag{8}$$

Together with $-\mathbf{k}_i$ they form a regular hexagon, so that they provide nontrivial couplings in the nonlinear term. The periodicity in flow direction is $4\pi/\sqrt{3}$, in the neutral direction it is 4π.

Finally, this hexagon is lifted upwards with $\mathbf{k}_1$ and $\mathbf{k}_2$ to form the remaining 12 vectors,

$$\begin{aligned}
&\mathbf{k}_7=\mathbf{k}_1+\mathbf{k}_4, \quad \mathbf{k}_8=\mathbf{k}_1+\mathbf{k}_5, \quad \mathbf{k}_9=\mathbf{k}_1+\mathbf{k}_6,\\
&\mathbf{k}_{10}=\mathbf{k}_1-\mathbf{k}_4, \quad \mathbf{k}_{11}=\mathbf{k}_1-\mathbf{k}_5, \quad \mathbf{k}_{12}=\mathbf{k}_1-\mathbf{k}_6,\\
&\mathbf{k}_{13}=\mathbf{k}_2+\mathbf{k}_4, \quad \mathbf{k}_{14}=\mathbf{k}_2+\mathbf{k}_5, \quad \mathbf{k}_{15}=\mathbf{k}_2+\mathbf{k}_6,\\
&\mathbf{k}_{16}=\mathbf{k}_2-\mathbf{k}_4, \quad \mathbf{k}_{17}=\mathbf{k}_2-\mathbf{k}_5, \quad \mathbf{k}_{18}=\mathbf{k}_2-\mathbf{k}_6.
\end{aligned} \tag{9}$$

The full set $\mathbf{k}_i$, $i=1\ldots18$ is shown in Fig. 1.

The Fourier amplitudes $\mathbf{u}(\mathbf{k}_i)$ have to be orthogonal to $\mathbf{k}_i$ because of incompressibility (2). If they are expanded in basis vectors perpendicular to $\mathbf{k}_i$, the pressure drops out of the equations and need not be calculated. We, therefore, chose normalized basis vectors,

$$\mathbf{n}(\mathbf{k}_i)=\left(\frac{-k_xk_z}{k_x^2+k_y^2},\frac{-k_yk_z}{k_x^2+k_y^2},1\right)^T \Big/ \sqrt{1+k_z^2/(k_x^2+k_y^2)},$$

$$\mathbf{m}(\mathbf{k}_i)=(k_y,-k_x,0)^T/\sqrt{k_x^2+k_y^2}, \tag{10}$$

so that $\mathbf{n}$, $\mathbf{m}$, and $\mathbf{k}$ form an orthogonal set of basis vectors. For the negative vectors $-\mathbf{k}_i$ we chose the basis vectors $\mathbf{n}(-\mathbf{k}_i)=\mathbf{n}(\mathbf{k}_i)$ and $\mathbf{m}(-\mathbf{k}_i)=-\mathbf{m}(\mathbf{k}_i)$. If the x and y components of $\mathbf{k}$ vanish, the above definitions are singular and replaced by

$$\mathbf{n}=(1,0,0)^T, \quad \mathbf{m}=(0,1,0)^T. \tag{11}$$

The Fourier amplitudes of the velocity are now expanded as

$$\mathbf{u}(\mathbf{k}_i,t)=\alpha(\mathbf{k}_i,t)\mathbf{n}(\mathbf{k}_i)+\beta(\mathbf{k}_i,t)\mathbf{m}(\mathbf{k}_i). \tag{12}$$

The impenetrable plates impose further constraints on the $\alpha(\mathbf{k}_i)$ and $\beta(\mathbf{k}_i)$. For $i=1$, 2, and 3, the wave vector has no components in the x and y directions, so that α and β have to be real. For $i=4$, 5, and 6, the velocity field cannot have any components in the z direction; hence, $\alpha=0$. The remaining wave vectors $\mathbf{k}_i$ and $-\mathbf{k}_i$ with $i=7,\ldots,18$, a total of 24, divide up into six groups of four vectors each,

$$\mathbf{k}=(k_x,k_y,k_z), \quad \mathbf{k}'=(-k_x,-k_y,k_z), \ -\mathbf{k} \text{ and } -\mathbf{k}'. \tag{13}$$

The groups are formed by the vectors and their negatives in the pairs with indices (7,10), (8,11), (9,12), (13,16), (14,17), and (15,18). The amplitudes of the vectors in the sets are related by

$$\begin{aligned}
\alpha(\mathbf{k})&=\alpha(-\mathbf{k})^*=-\alpha(\mathbf{k}')^*,\\
\beta(\mathbf{k})&=\beta(-\mathbf{k})^*=-\beta(\mathbf{k}')^*.
\end{aligned} \tag{14}$$

Thus the full model has $6+6+6\times4=36$ real amplitudes. Restricting the flow by a point symmetry around $\mathbf{x}_0=(0,0,\pi/2)^T$ eliminates the contributions from $\mathbf{k}_2$ and some other components, resulting in a 19-dimensional subspace with nontrivial dynamics and the following amplitudes:

$$\begin{aligned}
&\alpha(\mathbf{k}_1)=y_1, \quad \beta(\mathbf{k}_1)=y_2, \quad \alpha(\mathbf{k}_3)=y_3,\\
&\beta(\mathbf{k}_3)=y_4, \quad \beta(\mathbf{k}_4)=iy_5, \quad \beta(\mathbf{k}_5)=iy_6,\\
&\beta(\mathbf{k}_6)=iy_7, \quad \alpha(\mathbf{k}_7)=y_8, \quad \beta(\mathbf{k}_7)=y_9,\\
&\alpha(\mathbf{k}_8)=y_{10}, \quad \beta(\mathbf{k}_8)=y_{11}, \quad \alpha(\mathbf{k}_9)=y_{12},\\
&\beta(\mathbf{k}_9)=y_{13}, \quad \alpha(\mathbf{k}_{13})=iy_{14}, \quad \beta(\mathbf{k}_{13})=iy_{15},\\
&\alpha(\mathbf{k}_{14})=iy_{16}, \quad \beta(\mathbf{k}_{14})=iy_{17}, \quad \alpha(\mathbf{k}_{15})=iy_{18},\\
&\beta(\mathbf{k}_{15})=iy_{19};
\end{aligned} \tag{15}$$

components not listed vanish or are related to the given ones by the boundary conditions (14). A complete listing of the flow fields $\mathbf{u}_i$ associated with the coefficients y_i such that $\mathbf{u}=\Sigma_i y_i\mathbf{u}_i$ as well as of the equations of motion are available from the authors.

C. The equations of motion

In this 19-dimensional subspace $(y_1,\ldots,y_{19})$ the equations of motion are of the form

$$\dot{y}_i=\sum_{j,k} A_{ijk}y_jy_k-\nu K_iy_i+f_i. \tag{16}$$

Of the driving force all components but f_2 and f_4 vanish. Moreover, if the f's are taken to be proportional to ν, the resulting laminar profile has an amplitude independent of

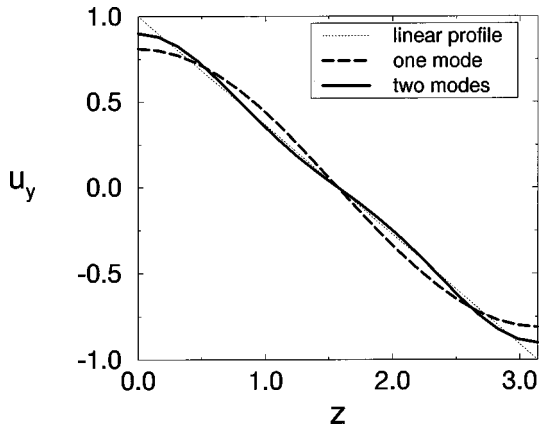

FIG. 2. The laminar profile in case of one or two driven modes; compare Eq. (17).

viscosity (and thus Reynolds number). These components give rise to a laminar profile that is a superposition of a $\cos(z)$ profile (from f_2) and a $\cos(3z)$ profile (from f_4). This allows us to approximate the first two terms of the Fourier expansion of a linear profile with velocity $u_y=\pm 1$ at the walls,

$$\mathbf{u}_0=\frac{8}{\pi^2}\left(\cos z+\frac{1}{9}\cos 3z\right)\mathbf{e}_y, \tag{17}$$

which can be obtained with a driving $f_2=4\nu/\pi^2$ and $f_4=4\nu/9\pi^2$ (see Fig. 2).

The nonlinear interactions in the Navier-Stokes equation conserve the energy $E=\frac{1}{2}\int dV\,\mathbf{u}^2$. In the 19-dimensional subspace, the corresponding quadratic form is

$$E=V\left(\sum_{i=1}^{7} y_i^2+2\sum_{i=8}^{19} y_i^2\right). \tag{18}$$

The above equations conserve this form without driving and dissipation. With dissipation but still without driving, the time derivative is negative definite, indicating a monotonic decay of energy to zero.

Finally, we define the Reynolds number using the wall velocity of the linear profile, $u_0=1$, the half width of the gap, $D=d/2=\pi/2$, and the viscosity ν,

$$\mathrm{Re}=u_0 D/\nu=\pi/2\nu. \tag{19}$$

The other geometric parameters are a period $4\pi/\sqrt{3}$ in flow direction and 4π perpendicular to it.

D. Symmetries

We achieved the impenetrability of the plates by requiring the mirror symmetry:

$$\begin{pmatrix} u_x \\ u_y \\ u_z \end{pmatrix}(x,y,-z)=\begin{pmatrix} u_x \\ u_y \\ -u_z \end{pmatrix}(x,y,z). \tag{20}$$

The reduction from 36 to 19 modes was achieved by restricting the dynamics to a subspace where the flow has the point symmetry around $\mathbf{x}_0=(0,0,\pi/2)^T$, a point in the middle of the shear layer,

$$\begin{pmatrix} u_x \\ u_y \\ u_z \end{pmatrix}(x,y,z+\pi/2)=\begin{pmatrix} -u_x \\ -u_y \\ -u_z \end{pmatrix}(-x,-y,-z+\pi/2). \tag{21}$$

In addition, there are further symmetries that can be used to reduce the phase space. There is a reflection on the y-z plane,

$$T_1:\begin{pmatrix} u_x \\ u_y \\ u_z \end{pmatrix}(x,y,z)\to\begin{pmatrix} -u_x \\ u_y \\ u_z \end{pmatrix}(-x,y,z), \tag{22}$$

and two shifts by half a lattice spacing,

$$T_2:\begin{pmatrix} u_x \\ u_y \\ u_z \end{pmatrix}(x,y,z)\to\begin{pmatrix} u_x \\ u_y \\ u_z \end{pmatrix}(x+2\pi,y,z), \tag{23}$$

$$T_3:\begin{pmatrix} u_x \\ u_y \\ u_z \end{pmatrix}(x,y,z)\to\begin{pmatrix} u_x \\ u_y \\ u_z \end{pmatrix}(x+\pi,y+\pi/\sqrt{3},z). \tag{24}$$

When applied to the flow, these transformations induce changes in the variables y_i (typically exchanges or sign changes), but the equations of motion are invariant under these transformations. Thus, if a certain flow has this symmetry, it leads to constraints on the variables y_i, and if it does not have this symmetry immediately a flowfield can be obtained by applying this symmetry transformation. We do not attempt to analyze the full symmetry structure here and confine our discussion to two illustrative examples, which are relevant for the stationary states discussed below. Demanding invariance of the flow field to the reflection symmetry T_1 leads to the following constraints on the variables y_i:

$$\begin{gathered} y_1=y_3=y_5=y_8=y_{15}=0, \\ y_6=y_7 \quad y_{10}=-y_{12}, \\ y_{11}=y_{13} \quad y_{16}=-y_{18} \quad y_{17}=y_{19}. \end{gathered} \tag{25}$$

The nonvanishing components, y_2, y_4, $y_6=y_7$, y_9, $y_{10}=-y_{12}$, $y_{11}=y_{13}$, y_{14}, $y_{16}=-y_{18}$, and $y_{17}=y_{19}$ thus define a nine-dimensional subspace.

For the combined symmetry T_1T_2 we find the constraints,

$$\begin{gathered} y_1=y_3=y_5=y_8=y_{15}=0, \\ y_6=-y_7 \\ y_{10}=y_{12}, \\ y_{11}=-y_{13} \quad y_{16}=y_{18} \quad y_{17}=-y_{19}, \end{gathered} \tag{26}$$

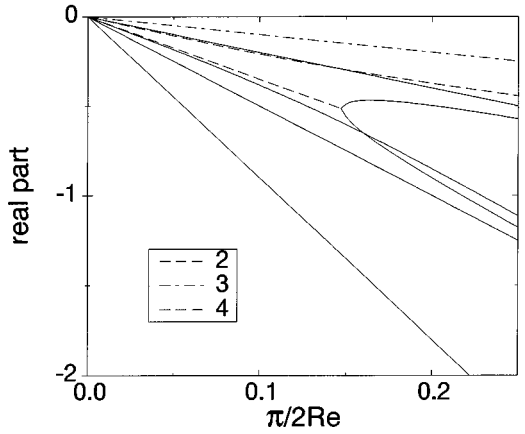

FIG. 3. Real parts of the eigenvalues of the linearized stability problem for one driven mode.

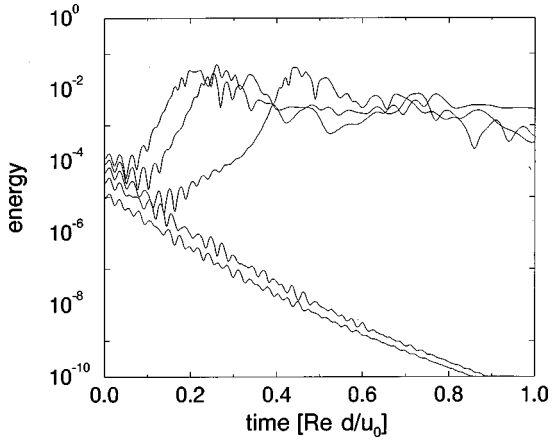

FIG. 4. The dynamics of perturbations for one driven mode at Re=400. The perturbation was selected randomly and scale by factors 3, 5, 7, 9, and 11, from bottom to top.

and again a nine-dimensional subspace with nonvanishing components y_2, y_4, $y_6=-y_7$, y_9, $y_{10}=y_{12}$, $y_{11}=-y_{13}$, y_{14}, $y_{16}=y_{18}$, and $y_{17}=-y_{19}$. The dimensions of the invariant spaces vary from a minimum of six (for each a T_1T_3 and $T_1T_2T_3$ invariance) to a maximum of ten (for T_2T_3 invariance).

As mentioned, one can classify flows according to their symmetries. The most asymmetric flows are eightfold degenerate as the application of the eight combinations of the symmetries give eight distinct flows. The laminar flow profile is invariant under all the linear transformations and is the only member of the class with highest symmetry. The other stationary states discussed below fall into equivalence classes with eight members or four members if they are invariant under T_1 or T_1T_2.

III. DYNAMICS OF PERTURBATIONS

A stability analysis shows that the laminar flow profile is linearly stable for all Reynolds numbers. The matrix of the linearization is non-normal with a block structure along the diagonal. To bring this structure out more clearly, it is best to order the equations in the sequence 1, 2, 3, 4, 5, 7, 15, 8, 9, 14, 13, 19, 12, 18, 6, 11, 17, 10, 16. The matrix of the linearization then is upper diagonal, with a clear block structure: there are ten eigenvalues isolated on the diagonal, three 2×2 blocks, and one 3×3 block as well as several couplings between them in the upper right corner. While some eigenvalues can be complex, all of them have negative real part as shown in Fig. 3. For vanishing viscosity, the eigenvalues become zero or purely imaginary.

Large amplitude perturbations, however, need not decay. Already in the linear regime the nonorthogonality of the eigenvectors can give rise to intermediate amplifications into a regime where the nonlinear terms become important [6–10]. In a related study on plane Couette flow [16] we used the lifetime of perturbations to get information on the dynamics in a high-dimensional phase space. As in that case, the amplitude of the velocity field in the z direction indicates the survival strength of a perturbation. Linearizing the equations of motion around the base flow $\mathbf{u}_0$ gives for the perturbation $\mathbf{u}'$ the equation

$$\partial_t\mathbf{u}' = -(\mathbf{u}_0\cdot\boldsymbol{\nabla})\mathbf{u}' - (\mathbf{u}'\cdot\boldsymbol{\nabla})\mathbf{u}_0 - \boldsymbol{\nabla}p' + \nu\Delta\mathbf{u}'. \quad (27)$$

The second term on the right-hand side describes the energy source for the perturbation, and depends, because of $\mathbf{u}_0 = u_0(z)\mathbf{e}_y$ and thus

$$(\mathbf{u}'\cdot\boldsymbol{\nabla})\mathbf{u}_0 = u_z'\partial_z u_0(z)\mathbf{e}_y \quad (28)$$

in an essential way on the z components of the perturbation. Thus, if the amplitudes y_8, y_{10}, y_{12}, y_{14}, y_{16}, and y_{18} become too small, the decay of the perturbation cannot be stopped any more. These modes account also for most of the off-diagonal block couplings. A model for sustainable shear flow turbulence has to include some of these modes.

We chose a fixed initial flow field with a random selection of amplitudes $y_1,\ldots,y_{19}$, scaled it by an amplitude parameter A, and measured the lifetime as a function of A and Reynolds number Re. Figure 4 shows the time evolution of such a perturbation at Re=400 with one mode driven and for different amplitudes. For small A there is an essentially exponential decay, whereas for larger amplitudes the perturbation swings up to large amplitude and shows no sign of a decline at all. The results for many amplitudes and Reynolds numbers are collected in Fig. 5 in a landscape plot. For small Reynolds number and/or small amplitude the lifetimes of perturbations are short, indicated by the light areas. For Reynolds numbers around 100 isolated black spots appear, indicating the occurrence of lifetimes larger than the integration time (which increases with Re so that $t_{\max}/\mathrm{Re}=4\pi$). The spottiness for Re between about 100 and 1000 is due to rapid changes in lifetimes from pixel to pixel. For Re above 1000 the long lifetimes dominate. These results are in good agreement with what has been observed in plane Couette flow. Figure 5(b) shows a similar plot for the case with two modes driven; it is qualitatively similar, but quantitatively shifted to higher Reynolds numbers.

In connection with the non-normality of the linearized eigenvalue problem it has been argued that the upper limit on the size of perturbations for which the nonlinear terms in the dynamics can be neglected decreases algebraically like $\mathrm{Re}^{-\alpha}$. Different exponents have been proposed, ranging from 1 to 3 [6,10,19]. It seems that for large Re (where the

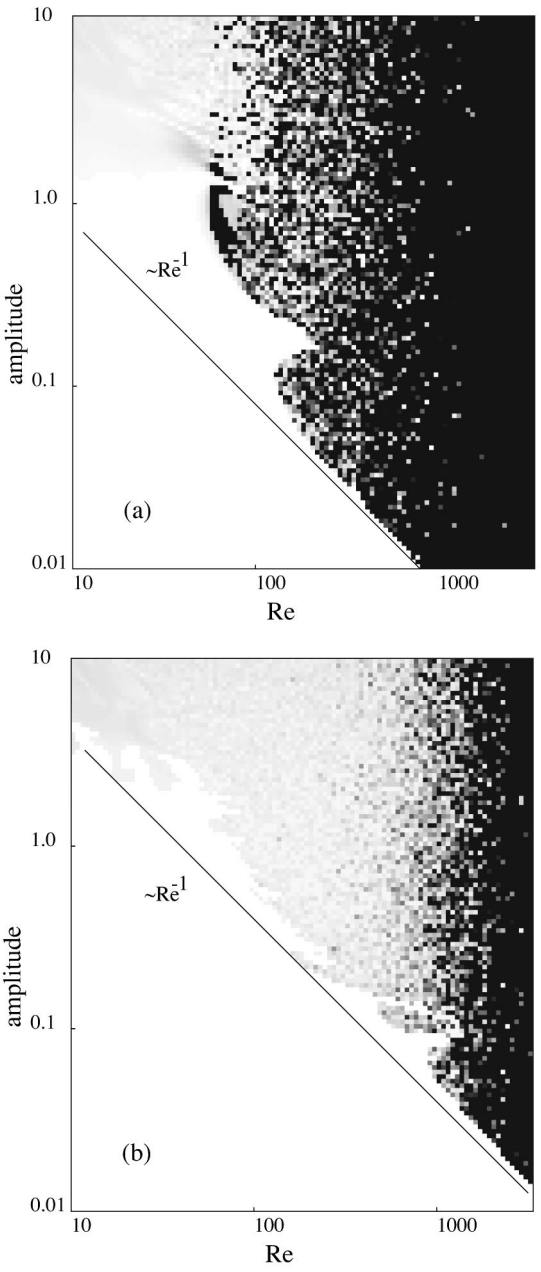

FIG. 5. Lifetime of perturbations as a function of amplitude and Reynolds number for the case of one driven mode (a) and two driven modes (b). The black regions correspond to lifetimes larger than $T=4\pi\cdot\mathrm{Re}$, the white regions to lifetimes shorter than $T/10$. The gray levels interpolate linearly between these levels.

model is actually less reliable because of the limited spatial resolution), the envelope of the long-lived states in the fractal lifetime plot decays like Re^{-1}.

The sensitive dependence of lifetimes on initial conditions and parameters is further highlighted in Figs. 6 and 7. The first shows the lifetime in the plane of the amplitudes y_{16} and y_{17} at Reynolds number $\mathrm{Re}=400$ with all other components fixed. There is considerable structure on many scales. One notes ''valleys'' of short lifetimes between ''plateaus'' of longer lifetimes and a granular structure within both. The striations are reminiscent of features seen near fractal basin boundaries [20]. Figure 7 shows successive magnifications of lifetime versus amplitude plots at $\mathrm{Re}=200$. Even after a

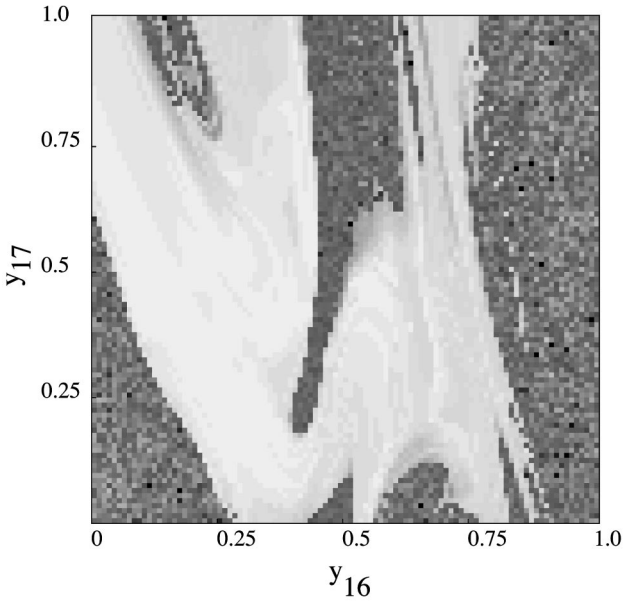

FIG. 6. Magnification of the fractal landscape of lifetimes as a function of the amplitudes y_{16} and y_{17} for the same perturbation as in Fig. 5 at $\mathrm{Re}=400$.

magnification by 10^7 there is no indication of a continuous and smooth variation of lifetime with amplitude.

IV. STATIONARY STATES

Motivated by the observation of stationary structures in plane Couette flow for sufficiently high Reynolds number

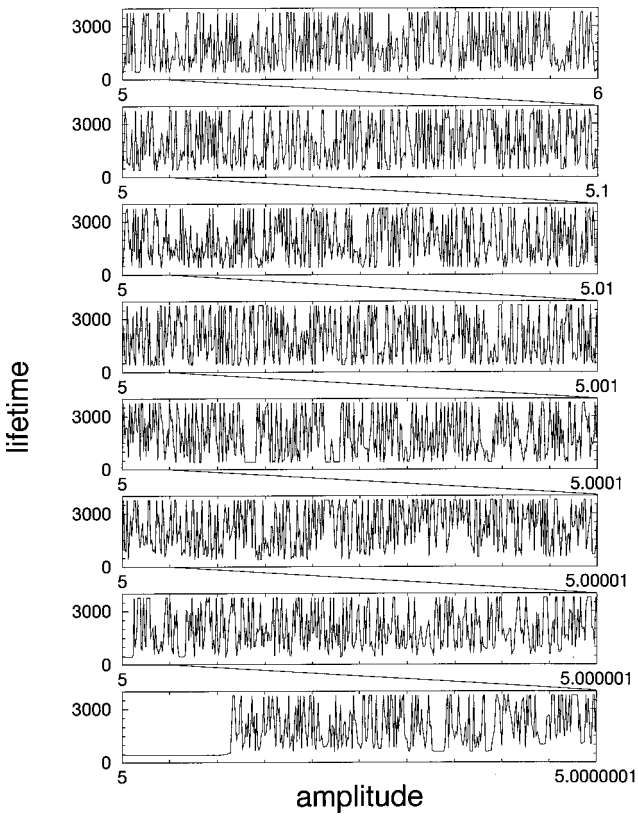

FIG. 7. Lifetimes of perturbations as a function of amplitude for the case of one driven mode at $\mathrm{Re}=200$ and successive magnifications by a factor of 10.

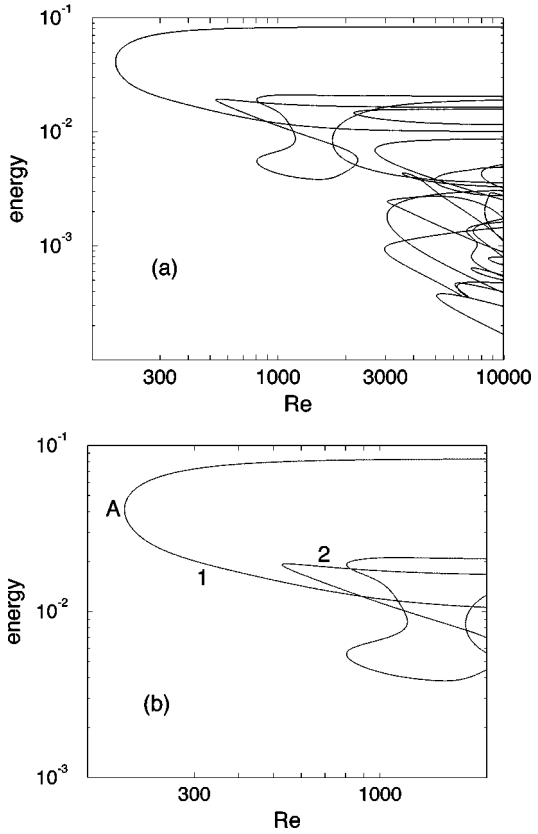

FIG. 8. Stationary states for a single driven mode (a) and a magnification (b) near the leading saddle node bifurcation near Re $=190$.

[12–14] we searched for nontrivial stationary solutions and studied their generation, evolution, and symmetries.

We computed the stationary states with the help of a Monte Carlo algorithm. The initial conditions for the y_i's were chosen randomly out of the interval $[-1/2,1/2]$ and the Reynolds number was chosen randomly matrix with an exponential bias for small Re in the interval [10,10 000]. With these initial conditions we entered a Newton algorithm. If the Newton algorithm converged, we followed the fixed point in Reynolds number as far as possible. We included about 200 000 attempts in the Monte Carlo search.

The stationary states found for a single driven mode are collected in Fig. 8. No stationary states (besides the laminar profile) were found for Reynolds numbers below about 190. Between 190 and about 500 there are eight stationary states, which divide into two groups of four symmetry-related states each. With increasing Reynolds number more and more stationary states are found and they reach down to smaller and smaller amplitude. The envelope of all states reflects the Re^{-1} behavior found for the borderline where nonlinearity becomes important. For two driven modes (Fig. 9) the situation is similar.

The appearance of the branches of the stationary states and, in particular, their coalescence near Re$=190$ suggests that the states are born out of a saddle-node bifurcation. And indeed, the eigenvalues as a function of Re show two eigenvalues moving closer together and collapsing at zero for Re $=190.41$ (Fig. 10). However, these eigenvalues are not the leading ones, so that one set of states has three unstable eigenvalues, the other two unstable ones. It is thus a

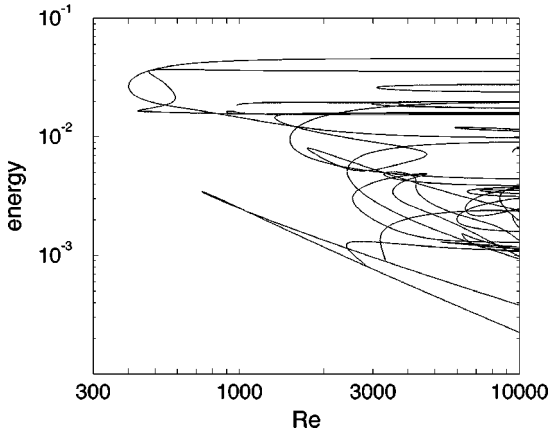

FIG. 9. Stationary states for two driven modes. Compared to Fig. 8 there seem to be more states and the next bifurcation is a lot closer to the leading one.

''saddle-node'' bifurcation into unstable states.

With increasing Re more and more stationary states appear, partly through secondary bifurcations, partly through additional saddle-node bifurcations. Their number increases rapidly with Reynolds number (Fig. 11) and this increase goes in parallel with the increase in density of long-lived states, Fig. 5. The detailed structure of the bifurcation diagram is rather complex and has not yet been fully explored. We note here that the various stationary states may be grouped according to their symmetries introduced in Sec. II D and that we found only stationary states, which belong to equivalent classes with four or eight members. The stationary states of the classes with four members are invariant under the transformation T_1 or T_1T_2. In addition, there are forward-directed bifurcations generating two branches with the same symmetry properties (eight- or four-member class) and inverse bifurcations of two branches belonging to eight-member equivalent classes. We also found a backward-directed bifurcation generating branches of an eight-member class, which is born out of a four-member class branch. The scenarios described above are marked in the bifurcation diagram, Fig.8.

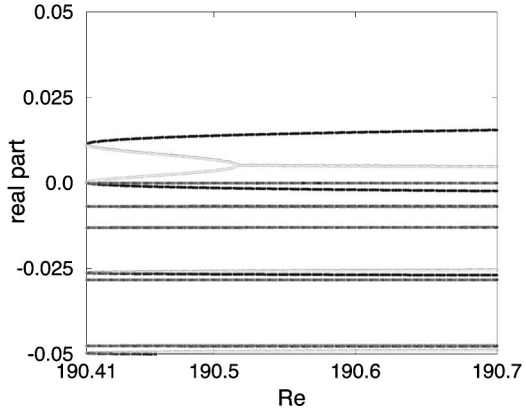

FIG. 10. Eigenvalues of the two branches of the stationary states *a* and *b* near the saddle-node bifurcation around Re$\approx$190. Note that indeed two eigenvalues with real positive and negative real parts at zero, but there are also eigenvalues with positive real part.

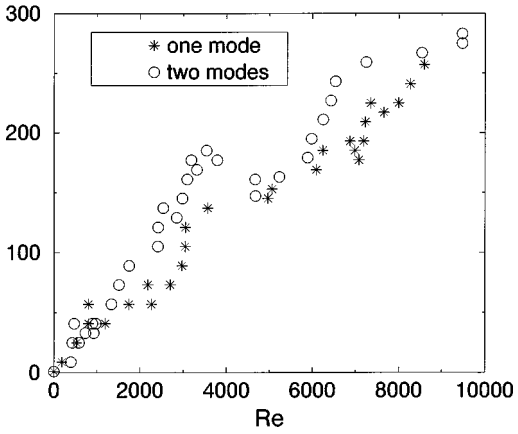

FIG. 11. Proliferation of stationary states for one and two driven modes.

V. CONCLUDING REMARKS

The few degrees of freedom shear model introduced here lies halfway between the simplest models of non-normality and full simulations. Its dynamics has turned out to be surprisingly rich. There are a multitude of bifurcations introducing stationary states besides the laminar profile; there are secondary bifurcations, and the distribution of lifetimes shows fractal structures on amazingly small scales. It seems that as one goes from the low-dimensional models [8,6] via the present one to full simulations one notes not only an increase in numerical complexity but also the appearance of qualitatively new features [21].

The simplest models with very few degrees of freedom focus on the non-normality of the linearized Navier-Stokes problem and emphasize the amplification of small perturbations. If the nonlinearity is included, a transition to another kind of dynamics, sometimes as simple as relaxation to a stationary point, is found [19].

Next in complexity are models like the one presented here that share with the few degree of freedom models the amplification and the transition but the additional degrees of freedom allow for chaos. When nonlinearities become important the dynamics does not settle to a fixed point or a limit cycle but continues irregularly for an essentially unpredictable time. The time is unpredictable because of the fractal lifetime distribution, which seems to persist down to amazingly small scale: tiny variations in Reynolds number or amplitudes of the perturbation can cause major variations in lifetimes. This fractal behavior is the new quality introduced by the additional degrees of freedom. Indications for this behavior are seen in the experiments by Mullin on pipe flow [22]. It is interesting to ask just how few degrees of freedom are necessary to obtain this behavior. Reducing our model to the T_1 subspace gives one with just nine degrees of freedom (comparable in number and flow behavior to the ones of Waleffe [10]) that still shows this fractal lifetime distribution. Further reduction, as in the four-mode model of [10], seems to eliminate them.

The full, spatially extended shear flows share essential features with the model but add new problems. Spatially resolved simulations of the present model [15] as well as plane Couette flow with rigid-rigid boundary conditions [12,14] show the occurrence of additional stationary states at sufficiently high Reynolds number that are unstable. An as yet unexplained feature in spatially extended plane Couette flow, which we believe to be connected to the high dimensionality of phase space, is the difference between Reynolds numbers where the first stationary states are born (about 125 in units of half the gap width and half the velocity difference) and the ones where experiments begin to see long-lived states (about 300–350) [23].

The fractal lifetime distributions have obvious similiarities to chaotic scattering [24,25,20]. Drawing on this analogy one would like to identify permanent structures in phase space away from the laminar profile that could sustain turbulence. This has partly been achieved by the search for stationary states. Many have been found but irritatingly only for Reynolds numbers above about 190 while long-lived states seem to appear much earlier. The solution to this puzzle must be periodic states and indeed we have found a few periodic states in a symmetry-reduced model at lower Reynolds numbers, close to the occurrence of the first long-lived states. This suggests that the dynamical system picture that long-lived states have to be connected to persistent structures in phase space is tenable.

There are several features of the model that can be studied further. In particular, quantitative characterizations of the fractal lifetime distribution, visualizations of the flow field, a detailed analysis of the primary and secondary bifurcation, and an investigation of the dependence on the aspect ratio of the periodicity cell are required and look promising. We expect the lessons to be learned from this simple model to be useful in understanding the dynamics of full plane Couette and other shear flows. Work along these directions continues.

[1] F.H. Busse, Rep. Prog. Phys. **41**, 1929 (1978).
[2] E. L. Koschmieder, *Bénard Cells and Taylor Vortices* (Cambridge University Press, Cambridge, England, 1993).
[3] C.D. Andereck, S.S. Liu, and H.L. Swinney, J. Fluid Mech. **164**, 155 (1986).
[4] S. Grossmann, in *Nonlinear Physics of Complex Systems*, edited by J. Parisi, S.C. Müller, and W. Zimmermann (Springer, Berlin, 1996), p. 10.
[5] P.G. Drazin and W.H. Reid, *Hydrodynamic Stability* (Cambridge University Press, Cambridge, England, 1981).
[6] T. Gebhardt and S. Grossmann, Phys. Rev. E **50**, 3705 (1994).
[7] L. Boberg and U. Brosa, Z. Naturforsch., A: Phys. Sci. **43**, 697 (1988).
[8] L.N. Trefethen, A. Trefethen, S. Reddy, and T. Driscoll, Science **261**, 578 (1993).
[9] F. Waleffe, Phys. Fluids **7**, 3060 (1995).
[10] F. Waleffe, Phys. Fluids **9**, 883 (1997).
[11] O. Dauchot and P. Manneville, J. Phys. II **7**, 371 (1997).
[12] M. Nagata, J. Fluid Mech. **217**, 519 (1990).
[13] M. Nagata, Phys. Rev. E **55**, 2023 (1997).

[14] R.M. Clever and F.H. Busse, J. Fluid Mech. **234**, 511 (1992); **344**, 137 (1997).
[15] F. Waleffe, Phys. Rev. Lett. **81**, 4140 (1998).
[16] A. Schmiegel and B. Eckhardt, Phys. Rev. Lett. **79**, 5250 (1997).
[17] B.F. Farrell and P.J. Ioannou, Phys. Rev. Lett. **72**, 1188 (1994).
[18] E.N. Lorenz, J. Atmos. Sci. **23**, 130 (1963).
[19] J.S. Baggett and L.N. Trefethen, Phys. Fluids **9**, 1043 (1997).
[20] E. Ott, *Dynamical Systems* (Cambridge University Press, Cambridge, 1994).
[21] B. Eckhardt, K. Marzinzik, and A. Schmiegel, in *A Perspective Look at Nonlinear Media in Physics, Chemistry, and Biology*, edited by J. Parisi, S.C. Müller, and W. Zimmermann (Springer, Berlin, 1998).
[22] A.G. Darbyshire and T. Mullin, J. Fluid Mech. **289**, 83 (1995).
[23] N. Tillmark and P.H. Alfredsson, J. Fluid Mecho **235**, 89 (1992); F. Daviaud, J. Hegseth, and P. Bergé, Phys. Rev. Lett. **69**, 2511 (1992).
[24] B. Eckhardt and H. Aref, Philos. Trans. R. Soc. London, Ser. A **326**, 655 (1988).
[25] B. Eckhardt, Physica D **33**, 89 (1988).